
STRUCTURE, PHASE TRANSFORMATIONS,
AND DIFFUSION

A Study about Ni–8 at % W Alloy Substrates Used for REBCO Coated Conductors

Yaotang Ji^a, Hongli Suo^{a, *}, Yichen Meng^a, Xinyu Wu^a, Kausar Shaheen^{a, c}, Lin Ma^a,
Min Liu^a, Lei Wang^b, and Zili Zhang^{b, **}

^a Key Laboratory of Advanced Functional Materials, Ministry of Education, College of Materials Science and Engineering, Beijing University of Technology, 100 Pingleyuan, Chaoyang District, Beijing, 100124 China

^b Institute of Electrical Engineering, Chinese Academy of Sciences, Beijing, 100190 China

^c Department of Physics, Jinnah College for Women, University of Peshawar, Peshawar, Khyber Pakhtunkhwa, 25120 Pakistan

*e-mail: honglisuo@bjut.edu.cn

**e-mail: zilizhang0816@vip.126.com

Received June 7, 2020; revised October 11, 2020; accepted October 24, 2020

Abstract—Ni–8 at % W alloy ingots were prepared using a spark plasma sintering technique. The evolution of the microstructure, cold-rolling texture, and recrystallization texture of the Ni8W alloy were studied using X-ray diffractometry and electron backscatter diffractometry techniques. The results revealed the strong influence of the initial grain size on the cube texture formation of the annealed substrates. A strong cube texture was obtained in substrates with finer initial grains. A brass-type rolling texture was formed in the final cold-rolled tape after cold rolling. The cold-rolled tape mainly consisted of S, brass, and a weak {110} <118> texture. The cube orientation nuclei did not have a nucleation advantage at the early stage of recrystallization. Large-scale twinning was exhibited in the cold-rolled microstructure at a high annealing temperature. The cube orientation and RD (rolling direction)-cube orientation textures, which transformed from the cube twin orientation and random orientation grains, were grown immediately at almost the same rate. The cube orientation and RD-cube orientation grains grew faster than other orientation grains throughout the whole grain growth process. Finally, a strong cube texture was obtained for the Ni–8 at % W substrate after an optimized annealing process.

Keywords: spark plasma sintering, cube texture, rolling, recrystallization annealing, Ni8W substrate

DOI: 10.1134/S0031918X21140118

1. INTRODUCTION

Since the discovery of REBa₂Cu₃O_{7-x} (REBCO: RE stands for rare metal elements) as a second-generation high-temperature superconductor (2G HTS), substantial efforts have been made to develop a high-current superconducting wire for technological applications [1, 2]. REBCO tape has a complex structure composed of alloy substrates, transition layers, superconducting layers, and protective layers. At present, there are two main routes for the preparation of REBCO tapes: rolling-assisted biaxially textured substrates (RABiTS™) [3–6] and ion beam assisted deposition (IBAD™) [7, 8]. The IBAD™ route involves a non-textured alloy substrate prepared using a physical method for the deposition of the texture transition layer in order to produce high-quality 2G tapes, but it has a higher cost. In comparison, the RABiTS™ route involves a textured alloy substrate, which can reduce processing complexity and lower the cost. Therefore, the RABiTS™ route is usually preferred because of its excellent application potential as

a means for producing cheaper second-generation tapes for electric cables [9]. As has been well known for decades, the cube texture in nickel is obtained after heavy cold rolling and subsequent annealing as the primary recrystallization texture. Presently, nickel alloy with 5 at % tungsten (Ni5W) is considered to be the preferred substrate material for REBCO tapes (CC) [10, 11]. However, the ferromagnetism and low strength of Ni5W hinder the wider applications of REBCO-coated conductors [12]. To suppress ferromagnetism and to enhance the strength of the NiW alloy substrate at moderate working temperature, a substrate with 10 at % of tungsten content is essential [13]. However, the stacking fault energy (SEF) of the alloy continually reduces with an increase in W content. A low SEF affects the microstructure of the NiW alloy, resulting in a decrease in the cube texture content in cold-rolled recrystallization annealing [14].

The preparation of alloy ingots includes smelting and powder metallurgy methods. Powder metallurgy methods can comparatively control the purity of the

ingot and size of the initial grains [15], thereby improving the content of cube texture within the substrate. In a study of Ni–W alloy substrates obtained by these methods of preparation, the recrystallization temperature of the strong cube texture formed within a Ni–7 at % W (Ni 7 W) [16] substrate that was prepared via powder metallurgy was found to be 300°C higher than that of a Ni–7.5 at % W [17] substrate obtained through a smelting method. This may be due to pores in the substrates prepared by the powder metallurgy method; these defects play a pinning role in grain boundary migration during the grain growth process. Advanced spark plasma sintering (SPS) technology can enable the rapid preparation of high-density alloy ingots [18], opening an advanced preparatory pathway for coated conductors via powder metallurgy. Previously, mid-to-high SEF Ni-based metal alloy substrates received the most attention for use with coated conductor substrates [19–21]. For low stacking fault energy (SFE), high W content NiW alloy basebands ($W \geq 8$ at % W) with strong cube texture substrates are preferred [22, 23]. To date, there have been no systematic studies on the deformation evolution mechanism, recrystallization texture, or the final cubic texture content within the substrate.

Therefore, efforts are still needed to optimize the treatment conditions for the improvement of texture quality in alloyed nickel tungsten substrate tapes. In this study, Ni–8 at % W (Ni 8 W) alloy substrates with strong cube texture content were prepared via SPS technology, with a detailed investigation of cold rolling and recrystallization behavior during the preparation process.

2. MATERIALS AND METHODS

2.1. Preparation of Super-High W Substrate

Alloys with the compositions of Ni8W (% mol ratio of Ni : W ~ 92 : 8) made by utilizing Ni (200 mesh, purity >99.99%) and W (200 mesh, purity >99.99%) powders were mixed in a planetary ball mill for 6 h under a protected atmosphere (Ar with 4 at % H₂). The high-energy ball mill was a Fritch P6 with a milling speed of ~150 rpm. The mixed powders were packed into a graphite mold then cold pressed under an axial pressure of 15 MPa. The cold-pressed ingot was sintered for 5 min at 800°C (with a heating rate of 100°C/min) under a pressure of 30 MPa using a Dr. Sinter™ spark plasma sintering system (SPS-3.2). After that, the as-sintered ingot was subjected to homogenization annealing. The initial ingots were cold-rolled with a pass deformation of 5% in order to obtain a cold-rolled strip with a final thickness of 0.08 mm, and the total deformation reached 99%. A two-step annealing process [24] was followed in order to obtain substrates with a strong cube texture. The heat treatment processes were performed in an Ar atmosphere with 4 at % H₂.

2.2. Characterization

An X-ray diffractometer (Bruker AXS D8 Advance, Cu target) was used to analyze and measure the deformation texture of the Ni8W alloy during rolling, and TexEval MFC application software was employed to calculate the pole figures and ODFs. The recrystallized texture of the substrate sample was characterized by a scanning electron microscope (JEOL JSM 6500F) equipped with an electron backscatter diffraction detector (EDAX), and OIMTSL6.1 orientation analysis software was used to analyze the texture and grain boundaries in detail. The microstructure of the ingot was observed using a metallurgical microscope (Zeiss Axio imager A2M). The HVS-1000 digital hardness tester was used to measure the hardness changes of the alloy during cold rolling and annealing. In this study, the maximum deviation orientation angle of the texture measured by X-ray diffractometry (XRD) and electron backscatter diffraction (EBSD) was adjusted to 15° and 10°, respectively.

3. RESULTS AND DISCUSSION

3.1. Effect of Initial Grain Size on Cube Texture Formation within Ni8W Alloy Substrate

Figure 1 shows the optical microscopy of the RD–ND cross-section of the initial ingot and deformation at 50% ($\epsilon_{vm} = 0.8$), 75% ($\epsilon_{vm} = 1.6$), and 87.5% ($\epsilon_{vm} = 2.4$) after three homogenization heat treatments (no. 1 1100°C for 24 h, no. 2 1100°C for 24 h + 1200°C for 5 h, no. 3 1200°C for 24 h). With the increase in rolling deformation, defects such as pores within ingots appear at the grain boundaries in the form of a distributed strip. Figure 1a shows a cross-sectional view of the ingot after homogenization at 1100°C for 24 h. Fine and uniform grains with many lamellar twins and an average size of ~20 μm were observed. The fine grains were elongated along the RD direction at ϵ_{vm} value ~0.8, as displayed in Fig. 1b. With a strain value of 1.6, (Fig. 1c), lamellar tissues were distributed parallel to the RD direction. Even at $\epsilon_{vm} = 2.4$ (Fig. 1d), the corroded interface was still parallel to the RD direction, and lamellar tissues were very close to each other. At this time, it is difficult to identify the rolling structure. Figure 1e shows a cross-sectional view of the ingot, homogenized at 1100°C for 24 h and then at 1200°C for 5 h. Thick crystal grains and a comparatively wider annealed twin structure were obtained. The average grain size of ~150 μm (seven times greater than Ingot no. 1) with no fine crystals was obtained, as shown in Fig. 1a. The spacing between the lamellar interfaces was significantly wider than the rolling structure within Ingot #1 under the same deformation. Even at ϵ_{vm} values of ~2.4 (Fig. 1h), the lamellar structure parallel to the RD direction was still clearly identified, and the spacing was two to three times greater than that of the fine crystal ingot at $\epsilon_{vm} \sim 1.6$ (Fig. 1c). A cross-sectional view of a billet homoge-

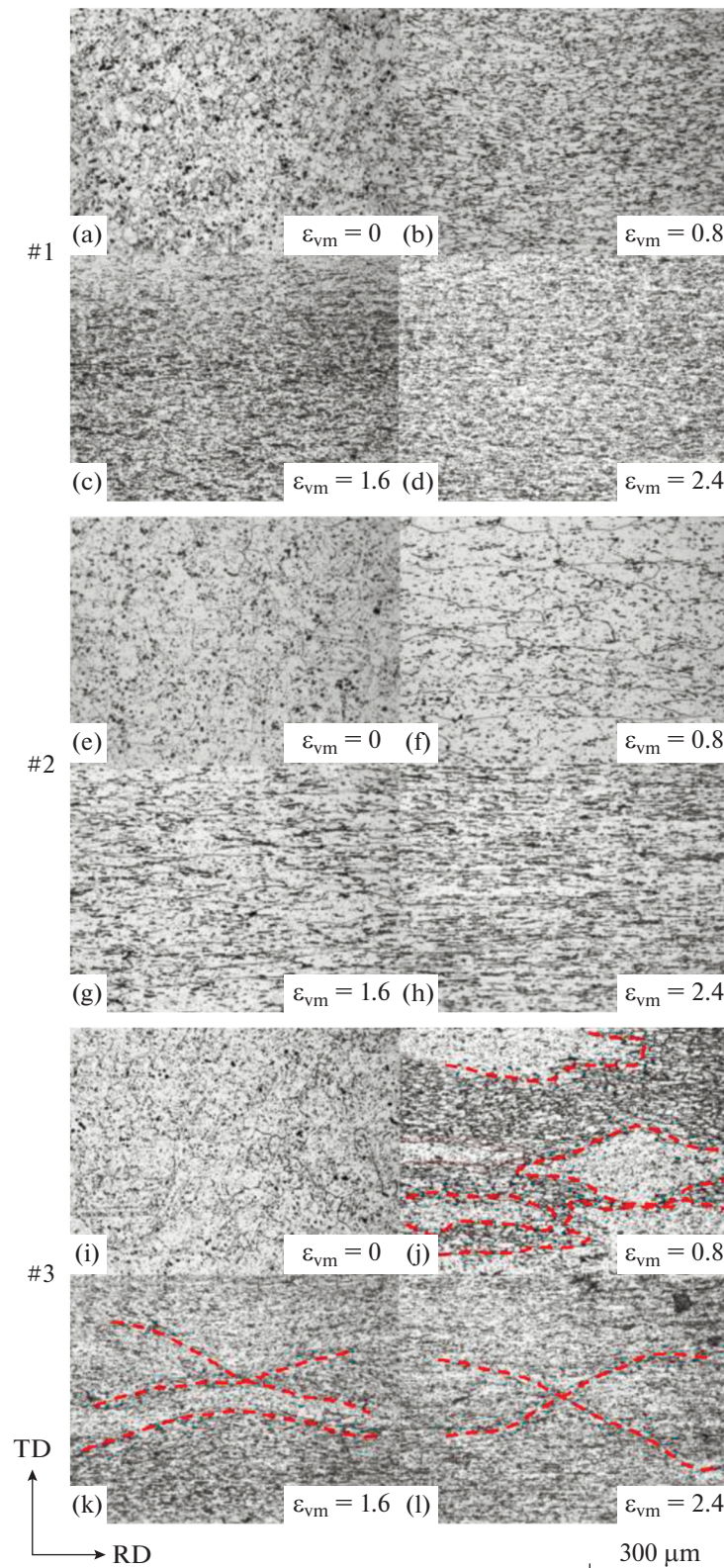


Fig. 1. Optical images of ingots with different initial grain sizes at various strain deformations. (a, e, i) $\epsilon_{vm} = 0$, (b, f, j) $\epsilon_{vm} = 0.8$, (c, g, k) $\epsilon_{vm} = 1.6$, (d, h, l), and $\epsilon_{vm} = 2.4$ annealed at (a) 1100°C for 24 h, (e) 1100°C for 24 h followed by 1200°C for 5 h, and (i) 1200°C for 24 h, (j) abnormal grains in dotted lines after 50% of deformed reduction; (k, l) shear bands observed after larger strain.

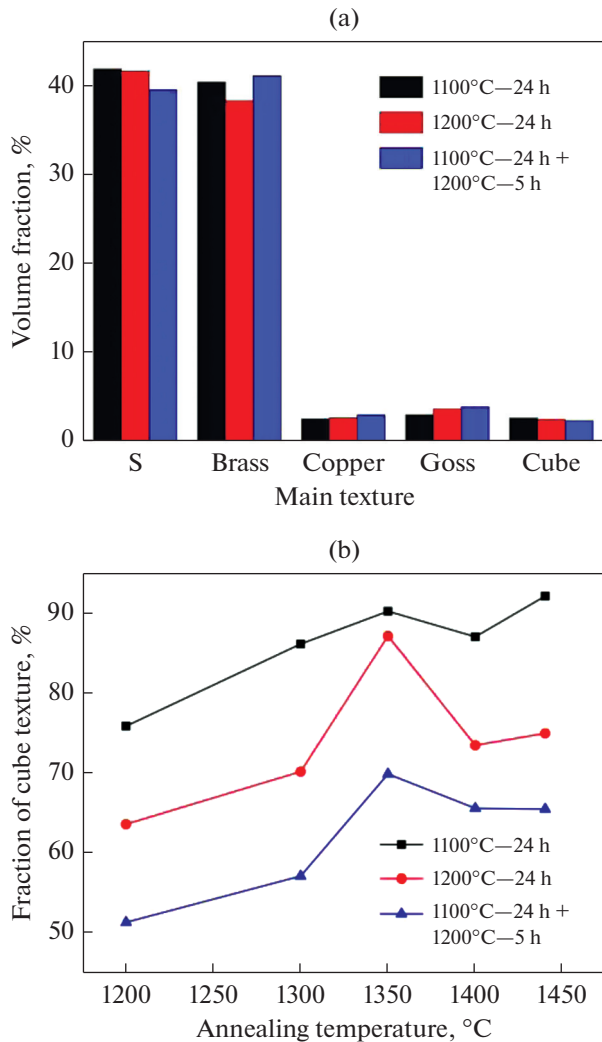


Fig. 2. (a) Fraction of main rolling components for as-rolled tapes (99% reduction) and (b) cube texture fraction on the surface of annealed substrates affected by annealing temperature.

nized at 1200°C for 24 h is shown in Fig. 1i. The grain morphology of Fig. 1i, simultaneously accompanied by fine grains and abnormally grown grains, was clearly different from Figs. 1a, 1e. The grains were unevenly distributed, with sizes ranging from 20 to 200 μm . During the subsequent rolling process, the coarse grains were not broken quickly but surrounded the fine grains along the rolling direction. A prominent shear was observed when the ϵ_{vm} value exceeded 0.8, as shown in Figs. 1k, 1l. The lamellar structure outside the shear band was similar to the fine-grained ingot structure under the same deformation during the cold rolling process.

As can be seen from Fig. 1, the average grain size for Ingot no. 2 was seven times greater than that of Ingot no. 1, but the deformation structure for both the ingots that were parallel to the rolling direction lacked

shear bands even after a large strain ($\epsilon_{\text{vm}} = 2.4$). Moreover, the spacing of the interface layer for Ingot no. 2 was five times wider than that of Ingot no. 1 at $\epsilon_{\text{vm}} = 2.4$. However, for Ingot no. 3 with abnormally grown grains, shear bands in the RD direction appeared even after a moderate strain ($\epsilon_{\text{vm}} = 1.6$). For Ingot no. 3 at low strain ($\epsilon_{\text{vm}} = 0.8$), the grains were abnormally grown along the RD into a uniform strip with an interface between the coarse fine grains. During the rolling process, the interface was subjected to larger shear stress, contributing to the uneven deformation. A shear structure under a larger strain gradually evolved owing to this uneven deformation area around the coarse-grained structure. The deformation texture has a very close relationship with the deformation mechanism of the material. The texture of the cold-rolled strip was finally measured via XRD, as shown in Fig. 2a. The S $\{123\}\langle 634 \rangle$, cube $\{001\}\langle 100 \rangle$, and brass $\{011\}\langle 211 \rangle$ texture in the cold-rolled strip prepared using ingot (a) were slightly stronger than those of Ingot no. 3, while the Goss $\{011\}\langle 100 \rangle$ texture was the lowest in all three ingots, but these differences were not very pronounced. The S orientation easily formed a large angle grain boundary at the $\langle 111 \rangle$ orientation with a high grain boundary migration rate, and the cube orientation grains were able to display growing advantages during recrystallization [25]. Therefore, the substrate obtained from Ingot no. 1 had the strongest cube texture (almost 90.2%, $< 10^\circ$), but it was not notably different from the substrate obtained from Ingot #3, as shown in Fig. 2b. Ingot no. 2 was relatively uniform coarse-grained with a lamellar structure under a larger strain. As shown in Fig. 2a, the S cube texture was the weakest within cold rolled strips prepared from Ingot no. 2, whereas the brass and Goss textures were the strongest. Although the difference in cold rolling texture was not very prominent compared to other cold rolling strips, the cube texture content was markedly lower (approximately 70%). The difference in the cube texture can be attributed to the broadening of the rolling deformation zone. Furthermore, it was difficult to find fine grains of less than 50 μm within Ingot no. 2, except for in the layered twinned structure. The fine deformation structure can have a higher grain boundary density and greater deformation energy storage of the material. Therefore, the driving force for recrystallization nucleation is greater, increasing the nucleation rate in the substrates [19].

3.2. Texture Evolution of Ni8W Alloy during Cold-Rolling

The ingot with homogenization heat treatment at 1100°C for 24 h, with the best texture performance after cold rolling and annealing, was further investigated for deformation and recrystallization. Figure 3a shows the hardness change curve of the cold-rolled strip with a total deformation of 99% (i.e. from 8 mm to 80 μm). A significant change in hardness was

observed at a strain value of 0.8. The hardness was increased linearly when ϵ_{vm} was increased from 0.8 to 4, but upon a further increase in ϵ_{vm} from 4 to 5.3, no significant change was observed in hardness. Finally, the hardness value ~ 464 HV (2.3 times higher than the original ingot) was obtained for cold rolled strip. The XRD pattern (with 2θ scanning range of 20° – 80°) for the cold-rolled strip under various strains is depicted in Fig. 3b. Three diffraction peaks for (111), (200), and (220) were observed at an angle of 44° , 51° , and 76° , respectively. With the increase in strain, the peaks at (111) and (200) were gradually decreased while the peak at (220) was increased.

The (111) pole maps of the rolling surface for Ni8W alloy at six different strains were investigated by XRD four-ring diffraction pattern, revealing the qualitative texture distribution of the material, as shown in Fig. 4. The increased concentration for Copper $\{112\}\langle 111 \rangle$ and S orientation was found when the ϵ_{vm} value was varied from 0.8 to 2.4. The maximum intensity for Copper texture was changed from 2.62 to 4.18. Upon further increase in strain up to 3.2, the Brass orientation tends to dominate the copper texture with the splitting of the highest intensity peak at both ends. At $\epsilon_{vm} = 4$, the highest intensity initially concentrated as the Copper orientation has now deviated towards the Brass orientation area. At $\epsilon_{vm} = 5.3$, a prominent Brass orientation intensity line has appeared, and finally a hybrid partial brass-type texture is obtained within the substrate. The previous [26] has proved that high-level fault energy for copper texture and low-level fault energy for brass texture is prominently obtained in the early stage of cold rolling with the deformation less than 50%. The copper texture is grown linearly with the increase in strain in metallic copper, while Copper texture in brass is slightly increased at the deformation level of 15% and begins to decrease at 30%. Ni8W alloy exhibits a mixed trend such as copper and brass texture at low and higher strains, respectively. Therefore, a mixed brass texture (involving both the copper and brass type) is finally formed, with the properties of low stacking fault energy and FCC (Face Center Cubic) structured material.

3.3. The Texture Evolution of Ni8W Alloy during Annealing

Figure 5 shows the fractions of main texture, grain boundaries, and average grain size of recrystallized grains of the Ni8W alloys treated at home temperatures of 700, 750, 800, 900, 1000, 1100, and 1200°C, without holding time at different temperatures. At a temperature of 700°C, a large number of S, brass, and randomly oriented rolling structures were found. The number of the cube and RD-cube $\{013\}\langle 100 \rangle$ orientation grains was basically the same, with the highest number of randomly oriented grains and almost zero $\Sigma 3$ twin boundaries. When the annealing temperature

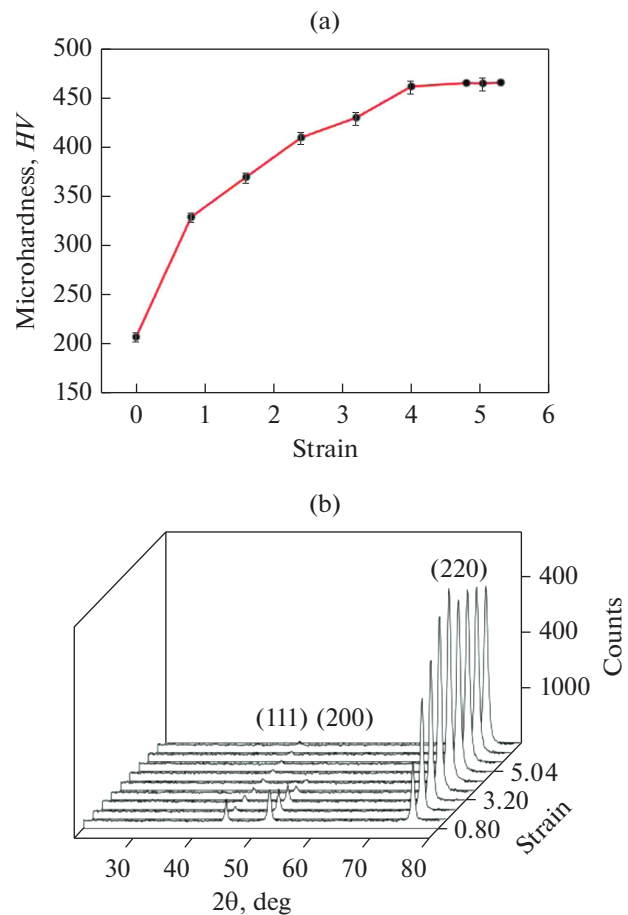


Fig. 3. (a) Hardness values under various strains, (b) XRD patterns of rolled Ni8W alloy with different strains determined on the rolling plane.

was increased to 750°C, the content of the three recrystallized textures, namely, the cube, RD-cube, C^T (Cube Twin) $\{122\}\langle 212 \rangle$ texture, and of random orientations increased with the rapid increase in large-angle grain boundaries and $\Sigma 3$ twin boundaries. Figure 6 shows the twin grain separated by $\Sigma 3$ twin boundaries with the adjacent recrystallized grain. During recrystallization for many metals, twinning is important for texture development that has been discussed in detail in a number of classic studies in this area, and the reader is referred to these studies for further details of the types of mechanisms involved [27–29]. At that time, the formation of C^T orientation grains was much greater than that of the cube and RD-cube orientation grains, but most of the grains were still small. The size of the cube and RD-cube orientation grains mainly ranged from 2–10 μm . Based on the theory of grain boundary migration [30], the grain boundaries in the $40^\circ \langle 111 \rangle$ orientation relationship had good migration capabilities. The ideal cube and S orientations had an orientation relationship of $\sim 48.6^\circ \langle 13\ 14\ 16 \rangle$, while the ideal RD-cube and brass

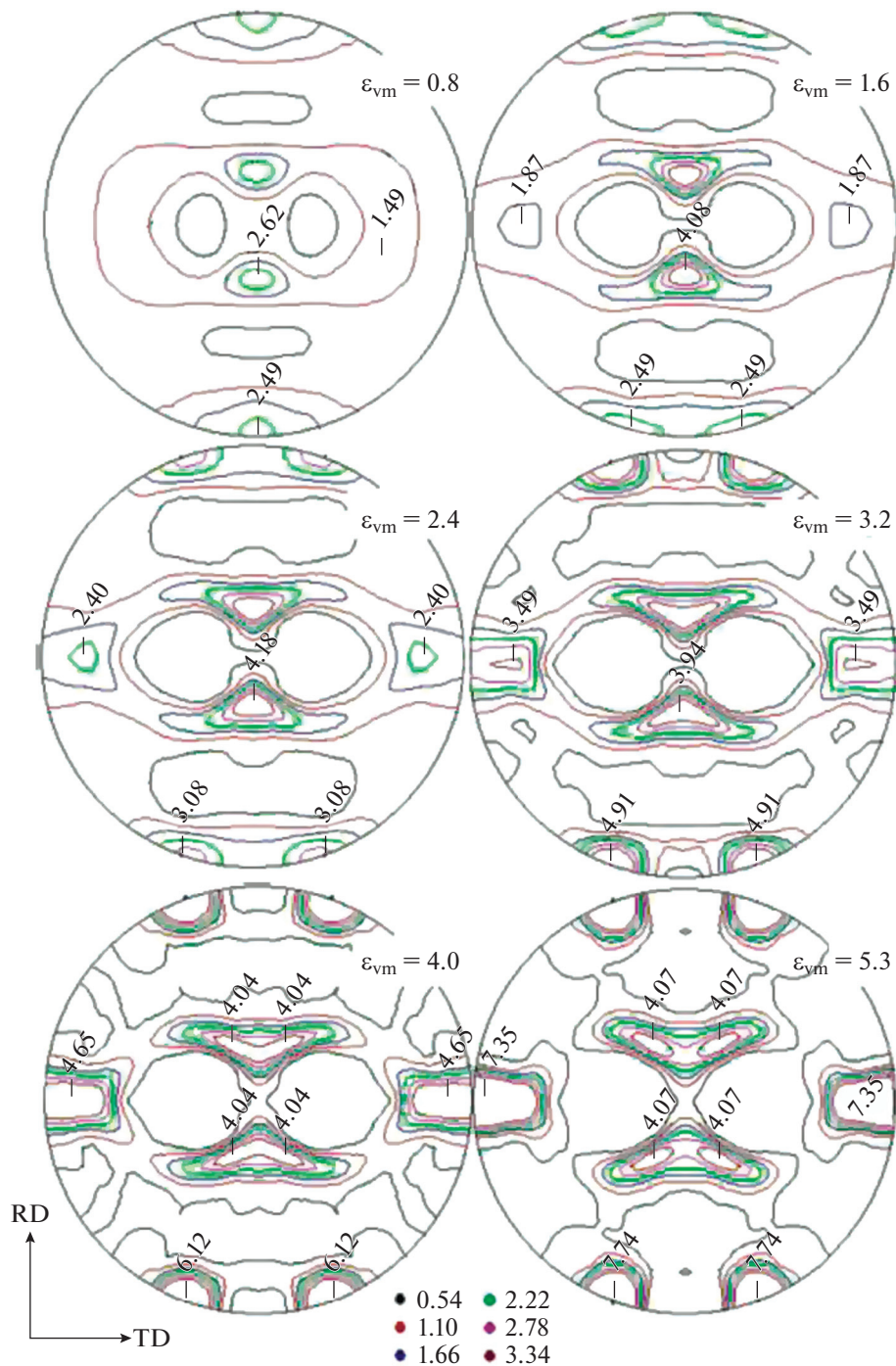


Fig. 4. (111) pole maps of as-rolled Ni 8 W alloy at different strains.

orientations had an orientation relationship of $\sim 44^\circ$ $\langle 578 \rangle$, close to the 40° $\langle 111 \rangle$ orientation, revealing a grain growth advantage compared to other orientation grains.

The complete recrystallization process was obtained at 800°C . The brass and S textures continuously weakened with a higher content of high-angle grain boundaries and randomly oriented grains. With

the progress in the twinning process, the content of twin boundaries continued to increase. Because of the further growth of RD-cube and cube orientation grains, most of the grain sizes ranged from 2–10 μm , with a significant increase in the number of grains. However, the number of grains in the C^T orientation significantly reduced, and the texture content also weakened. This is because the grains in the C^T orien-

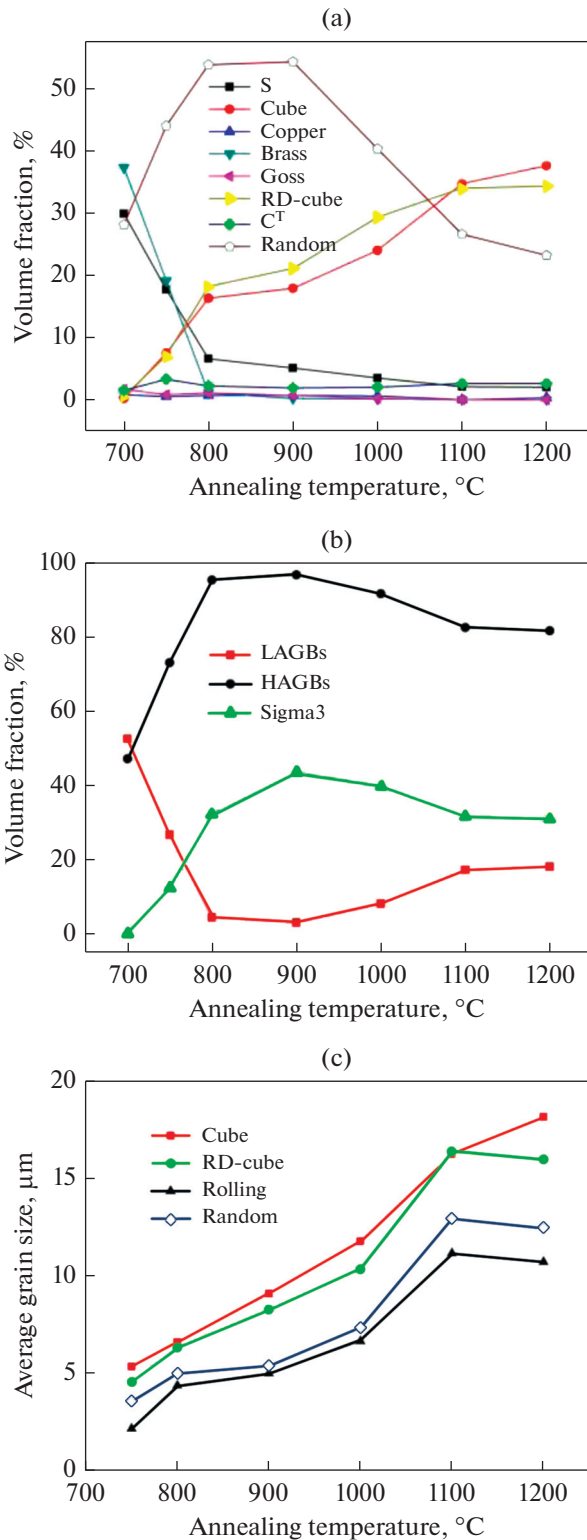


Fig. 5. (a) Fractions of main texture, (b) grain boundaries, and (c) average grain size of recrystallized grains of Ni8W alloys at different temperatures collected by EBSD.

tation were relatively small and were easily swallowed by surrounding grains because of the migration of high-angle grain boundaries. Although the content

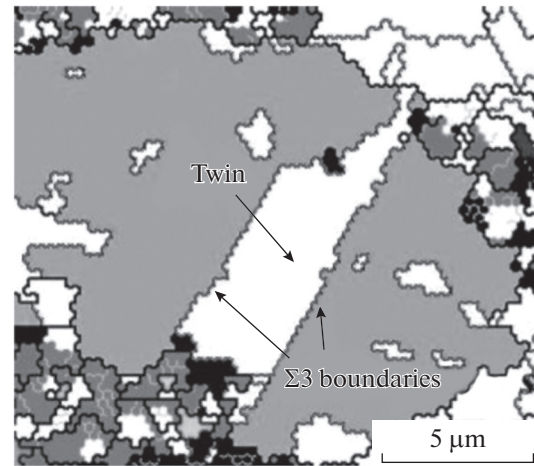


Fig. 6. EBSD maps of as-annealed Ni8W alloy determined on the surface at 750°C.

and number of randomly oriented grains were much larger than those of the RD-cube and cube orientations, the grain size was still much smaller than that of the RD-cube and cube orientations. When the annealing temperature was 1000°C, the cube, RD-cube, and randomly oriented grains continued to grow with a decreased number of grains. The number of C^T-oriented grains also decreased, but its growth was not very pronounced. The cube and RD-cube texture content continued to rise simultaneously, and the random orientation content began to decrease gradually. With the migration technique, the content of high-angle grain boundaries decreased with an increase in the low-angle grain boundary content. At an annealing temperature >1000°C, the content of cube and RD-cube texture was greater than the content of random orientation grains. The decreasing number of C^T and randomly oriented grains can also decrease the content of Σ3 twin boundaries. It is worth noting that although the number of RD cube orientation grains was greater than the cube orientation grains during the initial recrystallization, there were more fine grains in twin relationships with randomly oriented grains, which are absorbed during high-angle grain boundary migration. Therefore, the content of the cube and RD-cube texture is equivalent.

4. CONCLUSIONS

During the rolling process for ingots, various initial grain sizes lead to variations in the deformation and recrystallization texture of the substrate. The fine and uniform grain size of the initial ingot can be attributed to the stronger cube texture of the final substrate. A typical brass-type texture with a large deformation of ~99% were obtained within the Ni8W alloy substrate after the cold rolling process. In addition to the S texture, there is also a transition texture, <118>, between

the Goss and Brass orientation, but its strength is weak. During the early stage of recrystallization, cube-oriented crystal grains are formed by a large number of C^T orientation nucleus twins and are rapidly grown in a favorable orientation along with the S orientation deformation structure. The RD cube orientation grains are mainly formed due to a large number of randomly oriented nucleus twins and are grown with a brass orientation deformation structure. The substrate prepared via SPS technology was finally obtained with a strong cube texture (almost 90.2%) at a temperature of 1350°C.

FUNDING

This work was supported by the National Natural Science Foundation of China (51702316, 51807191 and 11745005), the General Program of Science and Technology Development Project of Beijing Municipal Education Commission of China (KM201810005010), 211 Program of Beijing City and Beijing University of Technology, and the Program of Top Disciplines Construction in Beijing (PXM2019_014204_500031) and the International Partnership Program of the Chinese Academy of Sciences (182111KYSB20170039), Youth Innovation Promotion Association of the Chinese Academy of Sciences (2020143).

REFERENCES

1. S. Ikeda, T. Motoki, S. Gondo, S. Nakamura, G. Honda, T. Nagaishi, T. Doi, and J. Shimoyama, "Synthesis of thick YBCO films up to 3.0 μm on metallic substrates by a fluorine-free metal organic decomposition method," *Supercond. Sci. Technol.* **32**, 1–6 (2019).
2. A. Sundaram, Y. Zhang, A. R. Knoll, D. Abraimov, P. Brownsey, M. Kasahara, G. M. Carota, R. Nakasaki, J. B. Cameron, G. Schwab, L. V. Hope, R. M. Schmidt, H. Kuraseko, T. Fukushima, and D. W. Hazelton, "2G HTS wires made on 30 μm thick Hastelloy substrate," *Supercond. Sci. Technol.* **29**, 1–6 (2016).
3. D. P. Norton, A. Goyal, J. D. Budai, D. K. Christen, D. M. Kroeger, E. D. Specht, Q. He, B. Saffian, M. Paranthaman, C. E. Klabunde, D. F. Lee, and B. C. Sales, "Epitaxial YBa₂Cu₃O₇ on biaxially textured nickel (001): an approach to superconducting tapes with high critical current density," *Science* **274**, 755–757 (1996).
4. M. W. Rupich, X. Li, S. Sathyamurthy, C. L. H. Thieme, K. DeMoranville, J. Gannon, and S. Fleshler, "Second generation wire development at AMSC," *IEEE Trans. Appl. Supercond.* **23**, 1–5 (2013).
5. Yu. V. Khlebnikova, D. P. Rodionov, I. V. Gervas'eva, T. R. Suaridze, and V. A. Kazantsev, "Conditions of sharp cube texture formation in thin tapes of Cu–Ni alloys for second-generation high-temperature superconductors," *Tech. Phys. Lett.* **41**, 341–343 (2015).
6. Yu. V. Khlebnikova, D. P. Rodionov, I. V. Gervas'eva, T. R. Suaridze, and L. Yu. Egorova, "Creation of a sharp cube texture in ribbon substrates of Cu–40% Ni–M (M = Fe, Cr, V) ternary alloys for high-temperature second generation superconductors," *Phys. Met. Metallogr.* **117**, 1129–1137 (2016).
7. Y. Iijima, N. Tanabe, O. Kohno, and Y. Ikeno, "In-plane aligned YBa₂Cu₃O_{7-x} thin films deposited on polycrystalline metallic substrates," *Appl. Phys. Lett.* **60**, 769–771 (1992).
8. S.-P. Hao, Y. Wang, H.-L. Suo, Q. Jia, M. Liu, and L. Ma, "Continuous electropolishing technique for long-length Hastelloy C-276 tape," *Rare Met.* **37**, 795–802 (2018).
9. S. Yoon, J. Kim, H. Lee, S. Hahn, and S. H. Moon, "26T 35 mm all-GdBa₂Cu₃O_{7-x} multi-width no-insulation superconducting magnet," *Supercond. Sci. Technol.* **29**, 1–6 (2016).
10. A. P. Malozemoff, "Progress in American Superconductor's HTS wire and optimization for fault current limiting systems," *Phys. C* **530**, 65–67 (2016).
11. D. Yu, L. Ma, H. L. Suo, J. Liu, Y. T. Ji, J. Cui, H. Tian, M. M. Gao, M. Liu, and Y. Wang, "The influence of tensile stress on the recrystallization and texture stability of Ni–5 at % W long tapes," *Phys. Met. Metallogr.* **120**, 570–577 (2019).
12. H. R. Kerchner, D. P. Norton, A. Goyal, J. D. Budai, D. K. Christen, D. M. Kroeger, E. D. Specht, Q. He, M. Paranthaman, D. F. Lee, B. C. Sales, F. A. List, and R. Feenstra, "Alternating current losses in biaxially textured YBa₂Cu₃O_{7-δ} films deposited on Ni tapes," *Appl. Phys. Lett.* **71**, 2029–2031 (1997).
13. Y. Zhao, H. Suo, Y. Zhu, M. Liu, D. He, S. Ye, L. Ma, R. Fan, Y. Ji, and M. Zhou, "Highly reinforced, low magnetic and biaxially textured Ni–7 at % W/Ni–12 at % W multi-layer substrates developed for coated conductors," *Supercond. Sci. Technol.* **21**, 1–6 (2008).
14. M. M. Gao, H. L. Suo, J. C. Grivel, Y. Zhao, P. K. Gao, M. Liu, and L. Ma, "Fabrication of the textured Ni–9.3 at % W alloy substrate for coated conductors," *IEEE Trans. Appl. Supercond.* **21**, 2969–2972 (2011).
15. J. H. Lim, K. T. Kim, H. J. Kim, J. Joo, W. Nah, G. W. Hong, J. G. Lee, and H. Mori, "Investigation of processing variables of Ni substrate for YBCO coated conductors," *IEEE Trans. Appl. Supercond.* **15**, 2679–2682 (2005).
16. Y. Zhao, H. Suo, Y. Zhu, J. C. Grivel, M. Gao, L. Ma, R. Fan, M. Liu, Y. Ji, and M. Zhou, "Study on the formation of cubic texture in Ni–7 at % W alloy substrates by powder metallurgy routes," *Acta Mater.* **57**, 773–781 (2009).
17. J. Eickemeyer, R. Huehne, A. Gueth, C. Rodig, H. Klauss, and B. Holzapfel, "Textured Ni–7.5 at % W substrate tapes for YBCO-coated conductors," *Supercond. Sci. Technol.* **21**, 1–8 (2008).
18. C. Shearwood, Y. Q. Fu, L. Yu, and K. A. Khor, "Spark plasma sintering of TiNi nano-powder," *Scr. Mater.* **52**, 455–460 (2005).
19. P. P. Bhattacharjee, R. K. Ray, and N. Tsuji, "Evolution of deformation and recrystallization textures in high-purity Ni and the Ni–5 at pct W alloy," *Metall. Mater. Sci. A* **41**, 2856–2870 (2010).
20. D. P. Rodionov, I. V. Gervas'eva, Yu. V. Khlebnikova, V. A. Kazantsev, and V. A. Sazonova, "NiCrM (M = W, Mo, V) ternary alloy tapes as cube-textured substrates

- for second-generation superconducting cables,” *Phys. Met. Metallogr.* **113**, 504–512 (2012).
21. D. P. Rodionov, I. V. Gervas’eva, Yu. V. Khlebnikova, V. A. Kazantsev, V. A. Sazonova, L. Yu. Egorova, and R. I. Gulyaeva, “Cubic texture of recrystallization of ribbon substrates made of nickel alloys alloyed with W, Mo, and Re refractory elements”. *Phys. Met. Metallogr.* **113**, 1079–1090 (2012)
 22. J. Eickemeyer, R. Hühne, A. Güth, C. Rodig, U. Gaitzsch, J. Freudenberger, L. Schultz, and B. Holzapfel, “Textured Ni–9.0 at % W substrate tapes for YBCO-coated conductors,” *Supercond. Sci. Technol.* **23**, 1–8 (2010).
 23. Y. T. Ji, H. L. Suo, L. Ma, Z. Wang, D. Yu, K. Shaheen, J. Cui, J. Liu, and M. M. Gao, “Formation of recrystallization cube texture in highly rolled Ni–9.3 at % W,” *Phys. Met. Metallogr.* **121**, 248–253 (2020).
 24. V. Subramanya Sarma, J. Eickemeyer, L. Schultz, and B. Holzapfel, “Recrystallisation texture and magnetisation behaviour of some FCC Ni–W alloys” *Scr. Mater.* **50**, 953–957 (2004).
 25. P. Gerber, J. Tarasiuk, and B. Bacroix, “Influence of the rolling reduction on static recrystallization in copper,” *Mater. Sci. Forum* **408–412**, 851–856 (2002).
 26. T. Leffers and R. K. Ray, “The brass-type texture and its deviation from the copper-type texture,” *Prog. Mater. Sci.* **54**, 351–396 (2009).
 27. A. Berger, P. J. Wilbrandt, F. Ernst, U. Klement, and P. Haasen, “On the generation of new orientations during recrystallization—recent results on the recrystallization of tensile-deformed fcc single-crystals,” *Prog. Mater. Sci.* **32**, 1–95 (1988).
 28. G. Gottstein, “Annealing texture development by multiple twinning in fcc crystals,” *Acta Metall.* **32**, 1117–1138 (1984).
 29. X. L. Li, W. Liu, A. Godfrey, D. J. Jensen, and Q. Liu, “Development of the cube texture at low annealing temperatures in highly rolled pure nickel,” *Acta Mater.* **55**, 3531–3540 (2007).
 30. G. Gottstein, D. A. Molodov, and L. S. Shvindlerman, “Grain boundary migration in metals: recent developments,” *Interface Sci.* **6**, 7–22 (1998).